Editors' Suggestion

Shape Deformation and Drag Variation of a Coupled Rigid-Flexible System in a Flowing Soap Film

Song Gao (高颂),[1,†] Song Pan (潘松),[1] Huaicheng Wang (王怀成),[1] and Xinliang Tian (田新亮)[1,2,*]
[1]State Key Laboratory of Ocean Engineering, School of Naval Architecture, Ocean and Civil Engineering, Shanghai Jiao Tong University, Shanghai 200240, China
[2]Shanghai Jiao Tong University Yazhou Bay Institute of Deepsea Technology, Sanya 572000, China

(Received 16 January 2020; revised 28 April 2020; accepted 24 June 2020; published 14 July 2020)

We experimentally study the soap film flow past a rigid plate with a trailing closed filament of a small bending modulus acting as a flexible afterbody. The complex fluid-structure interactions due to the deformable afterbody shape and corresponding dynamics are studied. We find that the shape of the afterbody is determined by filament length, filament bending modulus, and flow speed. A significant drag reduction of approximately 10.0% is achieved under specific conditions. We analyze the drag mechanism by characterizing the deformable afterbody shape. Our experiment and modeling suggest that such a flow control strategy and sizable drag reduction are expected to occur over a specific flow speed regime when a suitable flexible coating is added.

DOI: 10.1103/PhysRevLett.125.034502

Introduction.—Flow past a bluff body is encountered in numerous natural and industrial scenarios. The shape of the body, serving as the boundary for surrounding flow, dominates the fluid force and wake dynamics. Various flow controls [1], including drag reduction, lift enhancement, and vibration suppression, are achieved effectively by adjusting the shape of the bluff body, e.g., adding dimples [2] or a splitter plate [3–5]. For aquatic animals, the hydrodynamic performance is enhanced by the structural and morphological components of their bodies [6], e.g., riblets on shark skin [7] and bumps on whale flippers [8]. Bioinspired drag-reducing surfaces (or garments) have shown efficiency in improving athletes' performance [9]. However, these *passive* control methods require structural or surficial modifications of the rigid body. Flying birds tend to show elegant and deft ways to increase speed and reduce energy consumption. Their feathers self-adapt during flight, which is beneficial for aerodynamic performance [10–12]. The shape self-adaptation under flow, also referred to as *reconfiguration* [13,14], to reduce drag occurs universally in the botanic world as plants exhibit flexibility to bend, fold, and twist when subjected to fluid, both water [15] and air [16,17]. As a result, drag scales up more slowly than the classical drag∼velocity square law for a bluff body [18–20]. However, it seems impossible to make the shape or structure of cars or airplanes compliantly accommodate fluids in the real world. This raises a question of whether suitably adding a flexible coating to a rigid body can impart some favorable flow control features and improve its aero/hydrodynamic performance.

In this Letter, we experimentally investigate the two-dimensional (2D) flow past a rigid flat plate with a trailing closed filament with a negligible weight and small bending modulus. The filament is fully compliant with the flow and in turn controls the flow over the plate passively. A surprisingly reduced fluid drag is observed. This deformable afterbody is easily installed or removed and adjustable in size, enabling a simple and applicable flow control in various practical situations.

Experiments.—Soap films, which function as 2D flow tunnels, are convenient for studying 2D hydrodynamics in several respects [21–28]. In our vertically flowing soap film (soapy water density $\rho = 1.065\ \mathrm{g/cm^3}$), a rigid rod (length $L_p = 20$ mm; diameter 0.45 mm) serves as the flat plate placed normal to the incoming flow, and a flexible silk filament (length embedded in the soap film $L_d =$ 20–140 mm; diameter 12 μm; bending modulus $B = 3.43 \times 10^{-3}\ \mathrm{g \cdot cm^3/s^2}$; linear density $1.96 \times 10^{-6}\ \mathrm{g/cm}$) attached downstream behaves as the deformable afterbody. We use a dimensionless scale $\Lambda = L_d/L_p$ to describe the geometry of this rigid-flexible coupled system, where $\Lambda = 1$ corresponds to the situation without the trailing filament. The upper bound of Λ is approximately 7, beyond which stable and long-lasting flow cannot be achieved. In the parallel test section, a uniform velocity profile and constant film thickness are approached over 70% of the span about the midline. The tunnel is wide enough (tunnel width, 110 mm) that no

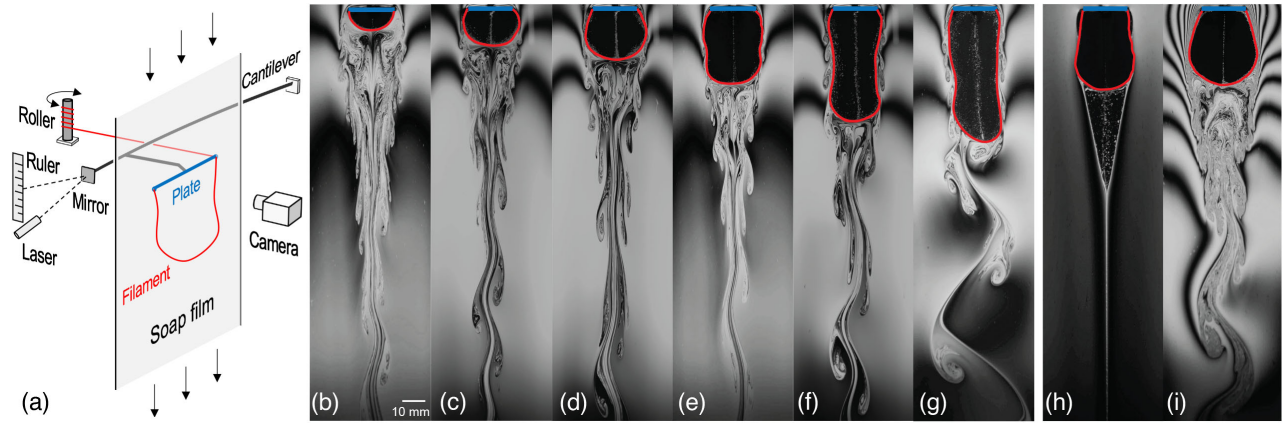

FIG. 1. (a) Schematic of the experiment: test section (not to scale). The plate and the filament are highlighted in blue and red, respectively. Typical flow features at $U = 1.45$ m/s are shown: (b) platelike regime, $\Lambda = 1.56$; (c),(d) cylinderlike regime, $\Lambda = 2.81$ and $\Lambda = 3.47$; (e) slender shape regime, $\Lambda = 4.25$; (f) rolling vortex regime, $\Lambda = 6.46$; and (g) flapping regime, $\Lambda = 6.95$. The other two cases, (h) $\Lambda = 4.26$ at $U_1 = 0.97$ m/s and (i) $\Lambda = 4.30$ at $U_7 = 1.90$ m/s, are comparable with (e) to show the influence of flow velocity U.

obvious blockage is observed. Wake patterns are visualized by an interference technique using the monochromatic light of a low-pressure sodium lamp. The fluid drag acting on the plate is obtained by measuring the vertical displacement of the supporting cantilever [19]. This method is proven to be both statically and dynamically reliable [29]. During the experiment, L_d can be modified gently and continuously without suspending or even disturbing the flowing film [30], as shown in Fig. 1(a). Seven different flow velocities U ranging from 0.97 to 1.90 m/s are tested, and approximately 180 sets of measurements for different Λ are conducted per U. Each drag data point is time averaged over 30 sec. The filament is wetted by the fluid and constrained in the plane of the film, and the deformable afterbody appears to bend only, without a measurable extension in length. The filament is much thicker than the soap film (thickness $f = 1$–3 μm); thus, no obvious inside-outside fluid exchange is observed. The fluid inside is always circulating but at a small velocity of $u \sim 10^{-2}$ m/s. The Marangoni wave speed [31] is considerably larger than the flow speeds, and thus no significant effects of compressibility are considered. The kinematic viscosity of the flowing soap film is $\nu = 0.07$ cm^2/s. The Reynolds number $\mathrm{Re} = L_p U/\nu$ is approximately 2700–5500.

Flow pattern.—Typical flow features at $U = 1.45$ m/s are illustrated in Figs. 1(b)–1(g). As shown in Fig. 1(b), the flow at $\Lambda = 1.56$ is almost identical to that for a 2D flat plate (not shown); i.e., the flow separates at the plate edges, and a pair of counter-rotating rings is formed at the rear of the plate. A very short closed filament only occupies some area of the wake, imposing no obvious influence on the ambient flow. Therefore, the first regime is denoted as the "platelike" (P) regime. As Λ increases, the flow plumps up the deformable afterbody at the edges of the plate; see Figs. 1(c) and 1(d). The incoming flow passes along the filament, and the separation occurs on the rear part of the deformable afterbody rather than at the plate edges. The significant separation delay observed here resembles the flow past a 2D cylinder [32], indicating the onset of the "cylinderlike" (C) regime. The width of the deformable afterbody in the C regime increases as Λ increases until the beginning of the "slender shape" (S) regime [Fig. 1(e)]. In the S regime, the middle section of the afterbody is squeezed by the outside fluid, yielding a narrow profile. In these regimes, the afterbody appears stationary and has reflectional symmetry about its midline, behaving like a rigid body. Beyond the S regime, flow enters the "rolling vortex" regime, where the afterbody shape is similar to that in the S regime but the filament traps significant vortex to roll along its sides [Fig. 1(f)]. Finally, when the filament is long enough, it flaps corresponding to the "flapping" regime [Fig. 1(g)].

Drag variation.—We further investigate the fluid drag acting on the coupled system to better understand the transitions. The fluid drag is normalized by the drag of the bare plate ($\Lambda = 1$) to show the drag variation at different U [Fig. 2(a)]. Additionally, the drag coefficient $C_D = \mathrm{Drag}/(\rho U^2 L_p f/2)$ is introduced to scale the fluid drag with flow velocity. The thickness of the soap film f is dependent on U as $f \propto U^{0.75}$ [33]. After taking this into account, we find all values of C_D gather together at approximately 2.0–2.1 at $\Lambda = 1$ [Fig. 2(b)], in agreement with the drag coefficient value for a 2D plate [34,35].

The drag curves show a similar tendency as Λ varies except $U_1 = 0.97$ and $U_2 = 1.17$ m/s. At these two small speeds, the afterbody shape deforms in a different way (shown in the next section), yielding different physics. Therefore, discussions on the drag will not consider these two cases in this Letter. The drag variation is closely related to the transitions; see Fig. 2(b). By increasing the filament length, the drag first decreases from the drag of a bare plate

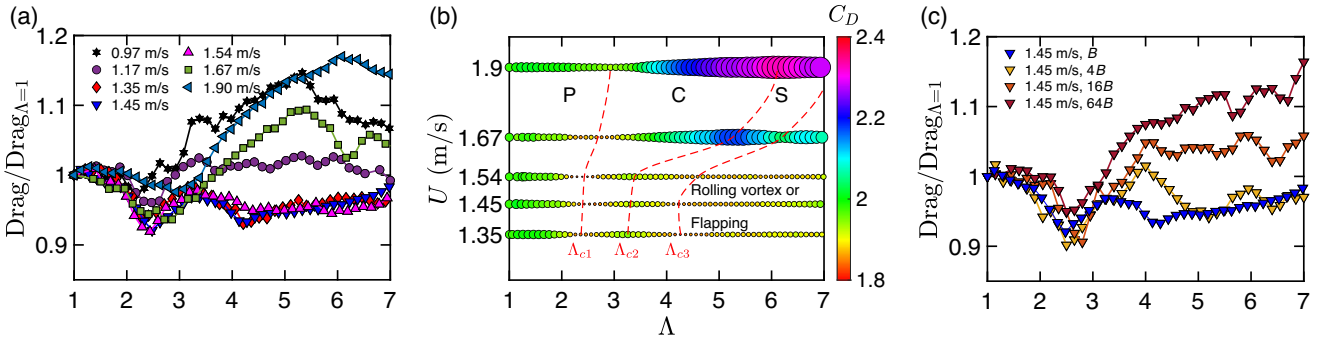

FIG. 2. (a) Fluid drag normalized by the drag of the bare plate is plotted vs Λ at different U. (b) Flow regimes in the $U-\Lambda$ map. Thresholds are obtained by the local minimum or maximum drag coefficient C_D. The color and size of the symbol both indicate the magnitude of C_D. (c) The fluid drag normalized by the drag of the bare plate is plotted vs Λ for four filaments with different bending moduli at $U = 1.45$ m/s.

until the first threshold at Λ_{c1}, where the onset of the C regime results in a local minimum drag. Then, the drag increases due to the growth of the afterbody width in the C regime until the second threshold at Λ_{c2}. After entering the S regime, the system benefits from its narrow shape and displays a second decrease in drag. However, when the S regime ends at Λ_{c3}, the rolling vortex on the sides and the flapping of the deformable afterbody reverse the trend, leading to a general increasing drag. It is difficult to explore the drag in these two regimes since the afterbody shape arbitrarily varies or the afterbody flaps strongly, making the soap film susceptible to rupture and large measurement fluctuations. The heavier drag burden suffered by the whole system distinguishes these two regimes from the previous three regimes. The curves of normalized drag at $U = 1.35$, 1.45 and 1.54 m/s collapse [Fig. 2(a)], and the critical Λ values are insensitive to speed for this range [$\Lambda_{c1} \approx 2.3$, $\Lambda_{c2} \approx 3.3$ and $\Lambda_{c3} \approx 4.2$ for all three speeds; see Fig. 2(b)]. Moreover, the most dramatic drag reduction over this range is observed at Λ_{c1}. Thus the range of $U = 1.35$–1.54 m/s is named the "favorable drag zone" (FDZ). Outside the FDZ, we observe the following: First, as U leaves the FDZ further, the normalized drag curves deviate more, which means using the bare plate drag to normalize drag regardless of the deformable shape of the afterbody has inherent limitations, especially when U is large (or small) enough to affect its shape significantly. Second, the C-S transition (occurs at Λ_{c2}) is delayed when U is higher; i.e., the shape of the filament preserves a "cylinder" at larger Λ when flow is faster.

We further investigate the effects of bending modulus of the filament. At $U_4 = 1.45$ m/s, experiments using three other filaments with bending moduli of $4B$, $16B$, and $64B$ are conducted. Bending modulus above $64B$ is not investigated due to the limitations of the experiment and filament material. Note that even $64B$ is still a small bending modulus compared with previous experimental studies on flexible bodies in a soap film [19,22,26,27]. As shown in Fig. 2(c), increasing bending modulus of the filament minimally alters the trend of drag variation, and the maximum drag reduction of approximately 10.0% is observed at Λ_{c1} for the filament with $4B$. However, the C-S transition is delayed as bending modulus increases; i.e., a stiffer filament preserves the shape of a cylinder till larger Λ at the same U. This is evident by noting that the stiffer filament resists bending by the fluid force component in the streamwise direction, which narrows its shape, corresponding to the onset of the S regime. A generally wider afterbody beyond Λ_{c1} is always observed for a filament with larger bending modulus, resulting in a larger drag. All these phenomena suggest that the drag force acting on the system is closely related to the shape of the deformable afterbody, which is determined by the length and bending modulus of the filament as well as flow velocity.

Shape deformation.—The shapes of the deformable afterbody at different Λ are shown in Figs. 3(a)–3(c). The average width of the afterbody $\overline{W}$ is calculated as the ratio of the enclosed area over the afterbody length L_{ds} (from the plate to the farthest downstream point). $\overline{W}$ shows a similar tendency for all speeds. As Λ increases, $\overline{W}$ first increases, corresponding to the P-C transition and the growth of the afterbody in the C regime. Then, $\overline{W}$ decreases as the flow transits to the S regime. Moreover, a larger speed results in an overall larger $\overline{W}$ at the same Λ, which is consistent with the phenomena observed in Figs. 1(e), 1(h) and 1(i).

To quantitatively study the afterbody shape, $\overline{W}/L_p$ is plotted versus Λ for different U in Fig. 3(d). All curves nearly collapse below $\Lambda \approx 2.3$, corresponding to the range of the P regime. Since the filament is short and trapped in the wake, its shape is not significantly influenced by the flow out of the separated free-shear layer. Beyond the P regime, the deformable afterbody tends to grow more in width at larger U, and the difference becomes more pronounced as Λ increases. Since there are no inside-outside fluid interactions and the inside velocity u is nearly two orders of magnitude smaller than that outside, the

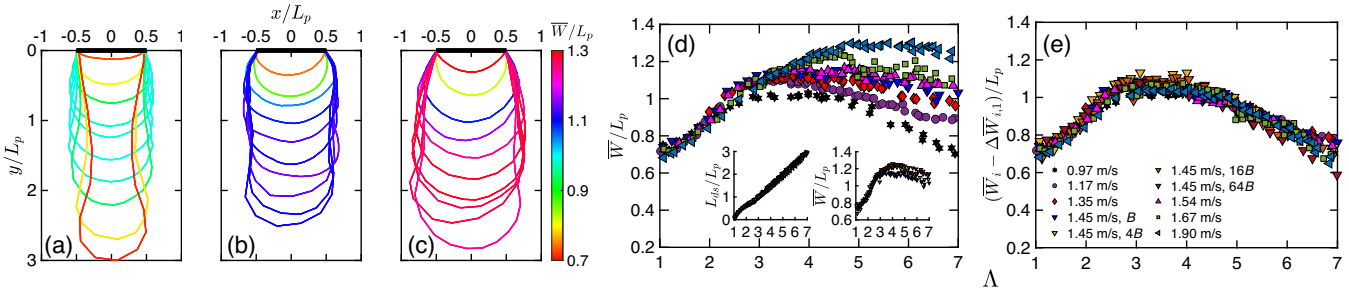

FIG. 3. Shape reconfiguration of the deformable afterbody as Λ varies at (a) $U_1 = 0.97$ m/s, (b) $U_5 = 1.54$ m/s, and (c) $U_7 = 1.90$ m/s. x and y are the spanwise and streamwise coordinates, respectively. The color of the filament indicates the average width of the afterbody, $\overline{W}/L_p$. (d) $\overline{W}/L_p$ is plotted vs Λ at different U. Left inset: L_{ds}/L_p vs Λ. Right inset: $\overline{W}/L_p$ vs Λ for four filaments with different bending moduli at $U = 1.45$ m/s, which is plotted separately for clarity. (e) The rescaling of $\overline{W}$ beyond Λ_{c1} using the model expressed by Eq. (1).

significant velocity difference causes a fluid pressure difference $0.5\rho(U^2 - u^2) \approx 0.5\rho U^2$ acting on the deformable afterbody. In the spanwise direction, this pressure difference acts on a length of the afterbody length L_{ds}, yielding a force that narrows or broadens the filament in its width. L_{ds} increases linearly as Λ beyond Λ_{c1} at a similar rate for all cases, i.e., $L_{ds} \approx c(\Lambda - \Lambda_{c1})$ [Fig. 3(d): left inset]. Furthermore, the filament with a larger bending modulus is wider at the same speed [Fig. 3(d): right inset]. Given any two different flow velocities U_i and U_j, the difference of the afterbody average width $\Delta\overline{W}_{i,j} = \overline{W}_i - \overline{W}_j$ at any Λ beyond Λ_{c1} can be written as

$$\Delta\overline{W}_{i,j} \approx 0.5kc\rho(B_m/B_n)^{\alpha}(U_i^2 - U_j^2)(\Lambda - \Lambda_{c1}), \quad (1)$$

where k is a constant fitting parameter with a value of 0.0188 cm $\cdot$ s^2/kg. B_m and B_n are the bending moduli for the filaments used under U_i and U_j, respectively. $\alpha = \pm 0.17$ shows the effect of bending modulus is weak. α is positive when $U_i > U_j$ and vice versa. If we subtract the width difference between U_i and U_1 (U_1 is chosen only for convenience), beyond Λ_{c1} using Eq. (1), all curves remarkably collapse on $\overline{W}_1$, as shown in Fig. 3(e). This model is capable of explaining the dominating physics underlying the width difference for all considered cases, although the method to fully resolve the afterbody shape and curvature at any given (Λ, U, B) has not been developed. Our model based on the pressure difference is helpful to explain the phenomena described previously. First, the C-S transition is delayed at higher speeds: the larger U is, the smaller the outside pressure. Thus, the afterbody tends to grow more in width, and the C regime lasts longer. Second, the physics at U_1 and U_2 differ: the afterbody shape is easily depressed at small U, and thus the separation points return to the plate edges [Fig. 1(h)], making the drag increase sharply [Fig. 2(a)].

Drag scaling based on the afterbody shape.—Since the afterbody width $\overline{W}$ is determined by Λ, B and U, using $\overline{W}$ as the characteristic length to normalize the drag gives more physical insights on the drag scaling. As shown in Fig. 4, all $C_{D,\overline{W}}$ curves nearly collapse over a wide range of Λ. Even the curves for higher U (or using filaments with larger B) are significantly closer to the cases in the FDZ compared with the previous scaling based on L_p [Figs. 2(a) and 2(c)], suggesting $\overline{W}$, which considers the reconfiguration of the afterbody is a reasonable characteristic length for this type of bluff body flow. More importantly, similar physics, including shape deformation and drag variation, are reasonably expected to occur at even larger Re regimes than the FDZ, although the drag reduction is not that significant. Thus, for moving rigid objects in the similar Re regime, with the addition of a suitable flexible coating (small bending modulus), similar drag reduction will occur. One should note that a larger discrepancy is observed beyond the S regime ($\Lambda > 4.2$) even for the FDZ cases. The possible reason is the contributions from the form drag and skin friction drag to the total drag change. In the previous study on bluff body flow in soap film [19], the form drag predominates due to the small upper bound of

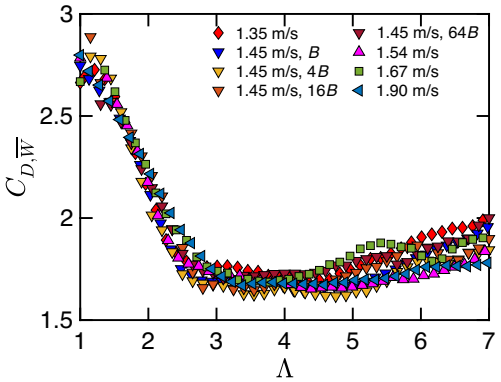

FIG. 4. The fluid drag is rescaled after taking the effects of shape deformation into account. A new drag coefficient $C_{D,\overline{W}}$, which is normalized using the characteristic length of $\overline{W}$, is plotted as a function of Λ at different U. The fluid drag of the filament with various bending modulus also observes this scaling law.

the estimated skin frictional drag [36,37]. However, for our coupled system, form drag is no longer the exclusively dominating force, especially in the rolling vortex and flapping regimes when the afterbody is long enough. A drag scaling law over all regimes can be proposed if the drag contribution can be better understood. Nevertheless, we explore the underlying physics of this new class of fluid-structure interactions and show the generalizability of this effective flow control method, which may inspire various novel designs benefiting the performance of athletes, race cars, diving submarines, and so on.

The authors acknowledge Yufeng Kou, Xia Wu, and Xiantao Zhang for assisting with the experiment. This work is supported by the Natural Science Foundation of Shanghai (Grant No. 19ZR1426300) and National Natural Science Foundation of China (Grant No. 11632011).

*Corresponding author.
tianxinliang@sjtu.edu.cn
†Present address: Department of Mechanical Engineering, Northwestern University, Evanston, Illinois 60208, USA

[1] H. Choi, W.-P. Jeon, and J. Kim, Annu. Rev. Fluid Mech. **40**, 113 (2008).
[2] P. W. Bearman and J. K. Harvey, AIAA J. **31**, 1753 (1993).
[3] A. Roshko, J. Fluid Mech. **10**, 345 (1961).
[4] P. W. Bearman, J. Fluid Mech. **21**, 241 (1965).
[5] E. A. Anderson and A. A. Szewczyk, Exp. Fluids **23**, 161 (1997).
[6] F. E. Fish and G. V. Lauder, Annu. Rev. Fluid Mech. **38**, 193 (2006).
[7] D. W. Bechert and M. Bartenwerfer, J. Fluid Mech. **206**, 105 (1989).
[8] E. A. van Nierop, S. Alben, and M. P. Brenner, Phys. Rev. Lett. **100**, 054502 (2008).
[9] J. Oeffner and G. V. Lauder, J. Exp. Biol. **215**, 785 (2012).
[10] J. Favier, A. Dauptain, D. Basso, and A. Bottaro, J. Fluid Mech. **627**, 451 (2009).
[11] J. Niu and D. L. Hu, Phys. Fluids **23**, 101701 (2011).
[12] S. Bagheri, A. Mazzino, and A. Bottaro, Phys. Rev. Lett. **109**, 154502 (2012).
[13] F. Gosselin, E. de Langre, and B. A. Machado-Almeida, J. Fluid Mech. **650**, 319 (2010).
[14] T. Leclercq and E. de Langre, J. Fluid Mech. **838**, 606 (2018).
[15] H. M. Nepf, Annu. Rev. Fluid Mech. **44**, 123 (2012).
[16] E. de Langre, Annu. Rev. Fluid Mech. **40**, 141 (2008).
[17] C. Cummins, M. Seale, A. Macente, D. Certini, E. Mastropaolo, I. M. Viola, and N. Nakayama, Nature (London) **562**, 414 (2018).
[18] S. Vogel, J. Exp. Bot. **40**, 941 (1989).
[19] S. Alben, M. Shelley, and J. Zhang, Nature (London) **420**, 479 (2002).
[20] M. Shelley and J. Zhang, Annu. Rev. Fluid Mech. **43**, 449 (2011).
[21] M. Rivera, P. Vorobieff, and R. E. Ecke, Phys. Rev. Lett. **81**, 1417 (1998).
[22] J. Zhang, S. Childress, A. Libchaber, and M. Shelley, Nature (London) **408**, 835 (2000).
[23] M. A. Rutgers, X. L. Wu, and W. B. Daniel, Rev. Sci. Instrum. **72**, 3025 (2001).
[24] P. Roushan and X. L. Wu, Phys. Rev. Lett. **94**, 054504 (2005).
[25] S. Jung, K. Mareck, M. Shelley, and J. Zhang, Phys. Rev. Lett. **97**, 134502 (2006).
[26] L. Ristroph and J. Zhang, Phys. Rev. Lett. **101**, 194502 (2008).
[27] L. B. Jia and X. Z. Yin, Phys. Rev. Lett. **100**, 228104 (2008).
[28] T. Schnipper, A. Andersen, and T. Bohr, J. Fluid Mech. **633**, 411 (2009).
[29] L. B. Jia and X. Z. Yin, Phys. Fluids **21**, 101704 (2009).
[30] The filament is fastened to one end of the plate, passed through a hook on the other end, and finally wrapped around a roller behind the film. The hooks are tiny and symmetric, and therefore, no obvious impact on the flow is observed. Since fluid forces always stretch the filament, rotating the roller smoothly increases or decreases L_d accordingly. The roller is rotated gently so that the bending of the cantilever is not influenced. Transverse motion of the reflected laser beam is not observed.
[31] Y. Couder, J. M. Chomaz, and M. Rabaud, Physica (Amsterdam) **37D**, 384 (1989).
[32] C. H. K. Williamson, Annu. Rev. Fluid Mech. **28**, 477 (1996).
[33] A. Sane, S. Mandre, and I. Kim, J. Fluid Mech. **841**, R2 (2018).
[34] A. Roshko, J Aeronaut. Sci. **22**, 124 (1955).
[35] B. R. Munson, T. H. Okiishi, W. W. Huebsch, and A. P. Rothmayer, *Fluid Mechanics* (Wiley, Singapore, 2013).
[36] P. W. Bearman, J. Fluid Mech. **28**, 625 (1967).
[37] G. K. Batchelor, *An Introduction to Fluid Dynamics* (Cambridge University Press, Cambridge, England, 1967).